Microsyst Technol (2013) 19:1441–1448
DOI 10.1007/s00542-013-1838-4

TECHNICAL PAPER

Simulation studies of contact sensor for disk defect mapping

Jin Liu · Junguo Xu · Jianhua Li

Received: 10 August 2012 / Accepted: 1 June 2013 / Published online: 16 June 2013

Abstract The keep increasing areal density in hard disk drive demands reducing the clearance between the read/write element and the disk surface. A clearance of 2 nm could be achieved using thermal-flying-height technology (Kurita et al. IEEE Trans Magn 41(5):3007–3009, 2005). In such a low-clearance flying regime, it is important to ensure the reliability of the head-disk interface. Head carbon overcoat wear should be taken into account and it requires ultra-smooth disk surface. Conventional method for disk inspection is using glide tester (Nayak et al. IEEE Trans Magn 39(2):729–734, 2003). However, with lower and lower clearance, some small defects on the disk surface can no longer be neglected, and these small defects cannot be detected by glide test. Thus a thermal-contact sensor integrated in a magnetic-head slider was proposed by Shimizu et.al to detect defects on disk surface (Shimizu et al. IEEE Trans Magn 47(10):3426–3432, 2011). Their experimental results confirmed that the contact sensor has equivalent sensitivity for detecting head-disk contact to that of a conventional acoustic emission sensor. And the defect mapping with this method was more sensitive than measurements with an optical surface analyzer. All these results were obtained using experimental method. Thus, numerical simulation studies are necessary in order to investigate the contact mechanics between asperities and the contact sensor. In this paper, a simplified contact model was developed to study contact mechanics between contact sensor and the disk asperity using finite element method. Different parameters' effect on the signal of a contact sensor was investigated. These results are of significance for the development of a thermal contact sensor in the hard disk drive for higher recording density.

J. Liu (✉)
Simulation and Mechatronics Laboratory, R&D Center, Hitachi Asia Ltd., Tampines Grande #08-01 Hitachi Square, Singapore 528736, Singapore
e-mail: kit_liujin@hotmail.com

Present Address:
J. Liu
Singapore HDD R&D Centre, a Western Digital company, Singapore, Singapore

J. Xu · J. Li
Japan Research Laboratory, Hitachi Global Storage Technologies Japan Ltd., Fujisawa, Japan

1 Modeling and materials

As illustrated in Fig. 1a, a small sensor is embedded near read/write element, and close to air bearing surface (ABS). When asperities on disk surface contact or slide along the sensor, friction will result in temperature increase in the sensor, thus asperities on disk surface could be detected.

Normally, the radius of TFC protrusion profile is about 10 mm, while the width of an asperity is only about 50–200 nm. When the asperity contacts and slides along TFC protrusion profile, it can be simplified as contacting a flat surface, as illustrated in Fig. 1b. The force applied by suspension loading force was illustrated as pressure exerted on slider top surface.

In the following simulations, the asperity is assumed to be a block, with height of 50 nm, width and length of w, as illustrated in Fig. 1b, and the contact sensor (CS) is of 1 μm in length and 0.04 μm in thickness. Table 1 lists materials' mechanical and thermal properties for the analyses.

2 Theory

According to the law of conservation of energy, when an object is pushed along a surface, the energy converted to

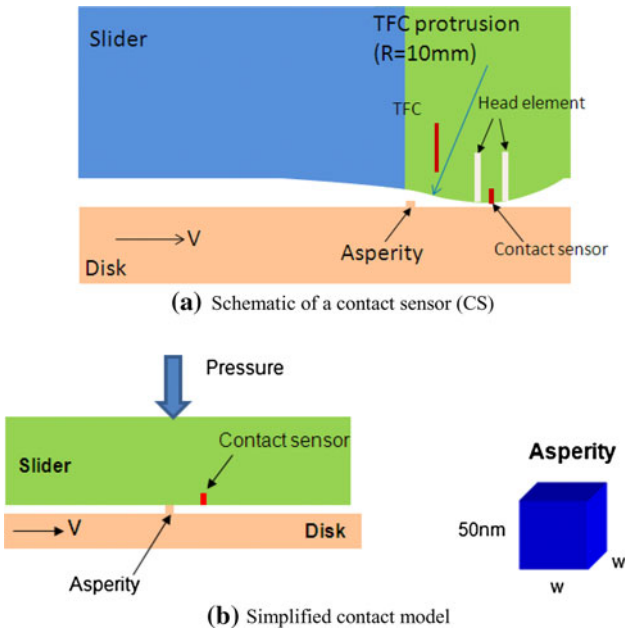

Fig. 1 Structural illustration of an asperity contacting contact sensor

Table 1 Materials' mechanical and thermal properties

Material	Young's modulus (Gpa)	Poisson's ratio	Coefficient of thermal expansion Xe-6 (K−1)	Thermal conductivity (W/mk)
Alumina (slider)	180	0.25	7.10	1.0
NiFe (ECS)	200	0.30	12.80	35
Aluminium alloy (disk)	140	0.30	2.42	1.0

heat is given by (Persson 2000; Barber 1967, 1970; ANSYS Inc 2009):

$$E_{th} = \mu \int F_n(x)dx \tag{1}$$

where F_n is the normal force, μ is the coefficient of kinetic friction, x is the coordinate along which the object transverses.

Supposing all frictional dissipated energy is converted into heat, heat due to contact between the slider and the asperity, q, per unit of nominal contact area A_n, per second is given by:

$$q = \frac{\mu F_n V}{A_n} = \mu P_n V \tag{2}$$

where P_n is the normal pressure, V is the sliding velocity and A_n is the normal contact area.

From Eq. (2), it is obvious that the heat generated by friction has linear relationship with friction coefficient, sliding velocity and applied normal pressure.

3 Simulation results

Some assumptions were made for the following analyses. (1) No overcoat was considered on both slider and disk surfaces. (2) No thermal contact conductance was considered unless specified. (3) Once contact happens, the asperity slides along the slider surface near the contact sensor, and the friction coefficient is taken to be 0.2 unless specified. (4) All dissipated energy is converted into heat, and half of the energy is transferred to contact (asperity) and target (slider) surfaces, respectively.

Surface-to-surface contact analyses were carried out to investigate parameters' effects on the temperature change in the contact sensor. The parameters may include: air bear cooling, normal pressure, asperity size, friction coefficient, sliding velocity, off-track and down-track, bias voltage applied to contact sensor and thermal contact conductance.

3.1 Air bearing cooling effect

Figure 2a shows the profiles of temperature change (averaging value of nodes at each time step) of the contact sensor with and without considering air bearing cooling effect. The asperity size w is 100 nm, normal pressure is taken to be 1 GPa and the sliding velocity is 10 m/s. In the figure, "W/ABS effect" means heat conduction was applied on air bearing surface (ABS) (convection coefficient = 1.9E + 6 W/m^{2}K) and "W/O ABS effect" means no heat conduction was applied on the ABS. In the analysis, the asperity keeps contacting slider surface from 3 μm ahead to 4 μm behind the contact sensor. Figure 2b illustrates the position of contact sensor and asperity with respect to time. It is shown that the asperity-sensor contacting time is about 0.014 μs.

From the Fig. 2a, it is observed that the temperature of the contact sensor increases quickly when the asperity starts to contact the sensor. After the asperity contacting the sensor, the temperature of the sensor gradually reduces. Compared to the case of "W/O ABS effect", the maximum temperature of the sensor reduces about 15 % for the case of "W/ABS effect". The ABS cooling effect was considered for the following analyses.

3.2 Normal pressure effect

Figure 3 shows effect of normal pressure on the temperature change of the contact sensor, where the asperity size w is 100 nm, and the sliding velocity is 10 m/s. Figure 3a is the temperature change profiles with time, and Fig. 3b is the relationship between applied pressure and the maximum temperature of the contact sensor. It is obvious that the maximum temperature of the contact sensor increases linearly with increasing normal pressure.

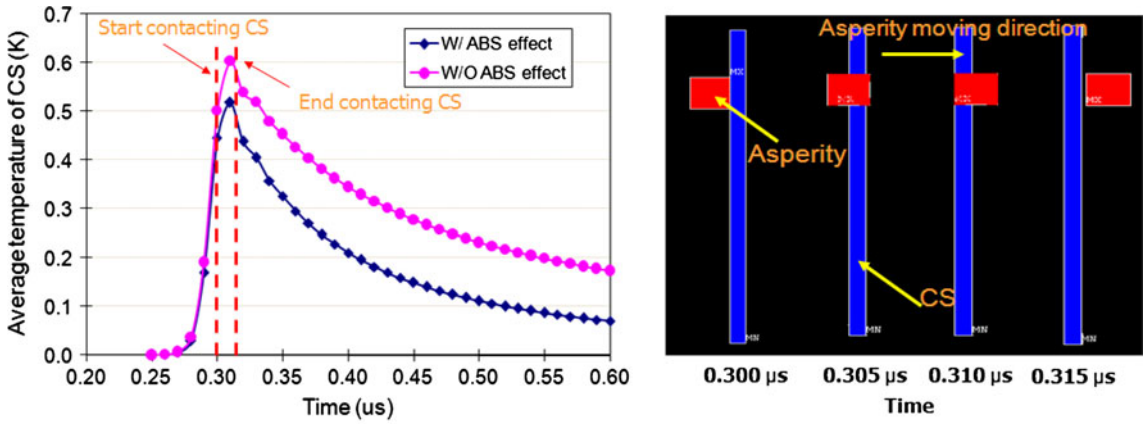

(a) Temperature profile for asperity contacting contact sensor (CS) **(b)** Position of CS/asperity vs time

Fig. 2 ABS effect on temperature change of contact sensor

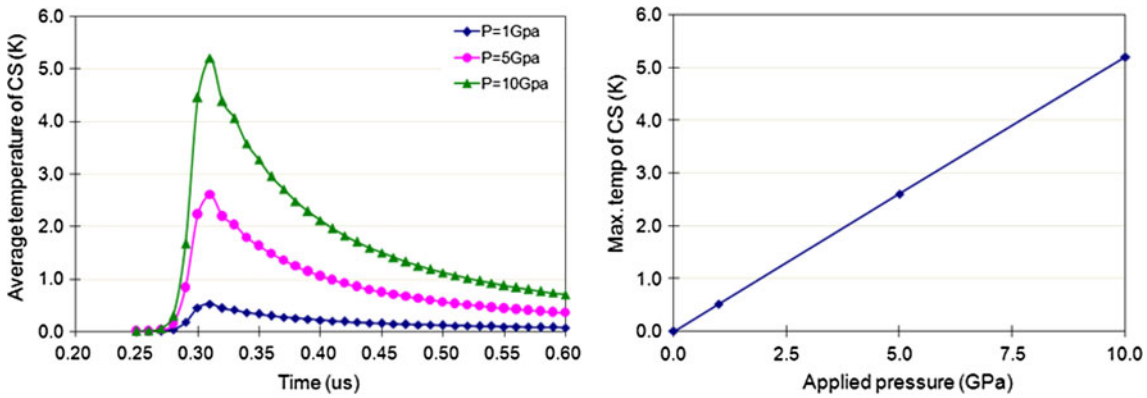

(a) Temperature profile **(b)** Pressure vs. temperature

Fig. 3 Normal pressure effect on the temperature change of contact sensor

3.3 Asperity size effect

Figure 4 shows effect of asperity size on the temperature change of the contact sensor, where the normal pressure is 5 GPa, and the sliding velocity is 10 m/s. Figure 4a is the temperature change profiles vs. time, and Fig. 4b is the relationship between the asperity area and the maximum temperature of the contact sensor. It is obvious that the maximum temperature of the contact sensor increases linearly with increasing asperity area.

3.4 Friction coefficient effect

Figure 5 shows effect of friction coefficient on the temperature change of the contact sensor, where the normal pressure is 5 GPa, and the sliding velocity is 10 m/s. Figure 5a is the temperature change profiles with time, and Fig. 5b is the relationship between friction coefficient and the maximum temperature of the contact sensor. It is obvious that the maximum temperature of the contact sensor increases linearly with increasing friction coefficient.

3.5 Sliding velocity effect

Figure 6 shows effect of asperity's sliding velocity on the temperature change of the contact sensor, where the normal pressure is 5 GPa. Figure 6a is the temperature change profiles with time, and Fig. 6b is the relationship between sliding velocity and the maximum temperature of the contact sensor. It is shown that the maximum temperature of the contact sensor increases with increasing sliding velocity. However, when the velocity increases to above 20 m/s, the maximum temperature of the contact sensor approaches to be a constant of 3 K. From Eq. (1), the temperature change of the contact sensor should have a linear relationship with the sliding velocity. This deviation is because that the contacting time between the asperity and the contact sensor increases with slower velocity, as

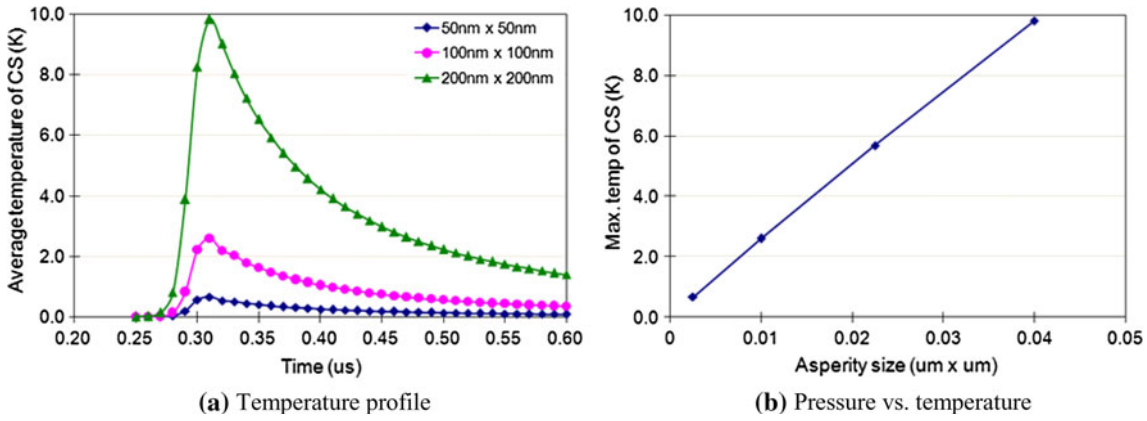

(a) Temperature profile **(b)** Pressure vs. temperature

Fig. 4 Asperity size effect on the temperature change of contact sensor

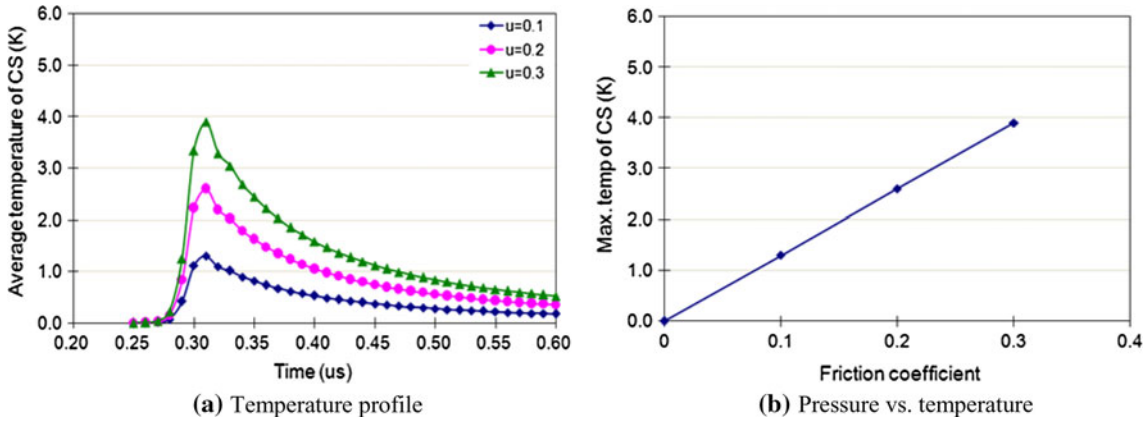

(a) Temperature profile **(b)** Pressure vs. temperature

Fig. 5 Friction coefficient effect on the temperature change of contact sensor

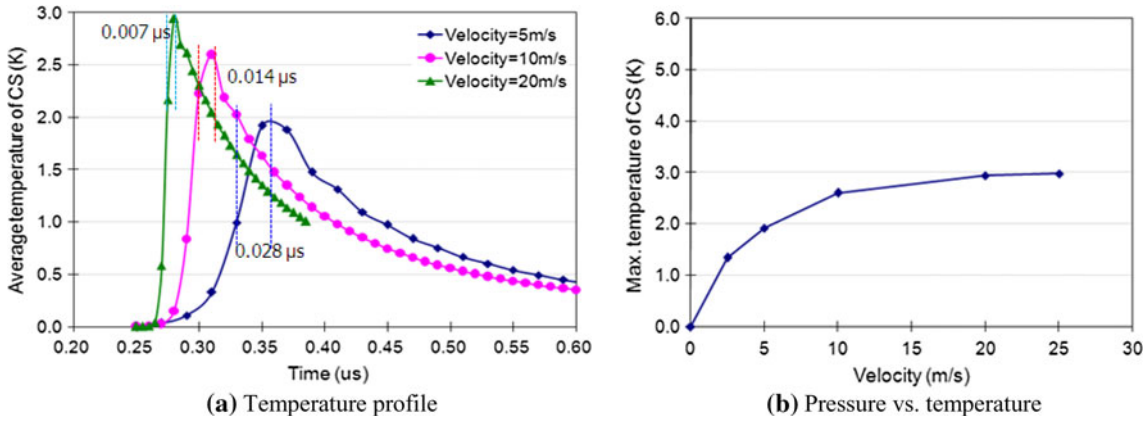

(a) Temperature profile **(b)** Pressure vs. temperature

Fig. 6 Sliding velocity effect on the temperature change of contact sensor

can be observed in Fig. 6a. With velocity higher than 20 m/s, the contact sensor is unable to respond to the quick increase of the heat energy furthermore.

3.6 Bias voltage effect

Normally, a bias voltage is applied to the contact sensor, it is necessary to investigate the bias voltage's effect on the temperature change in the contact sensor. Figure 7 shows the temperature change of the contact sensor with different bias voltage. It is shown the bias voltage effect is negligible.

3.7 Off-track effect

As we may know, the asperity may not always be able to contact the contact sensor directly. It is necessary to study

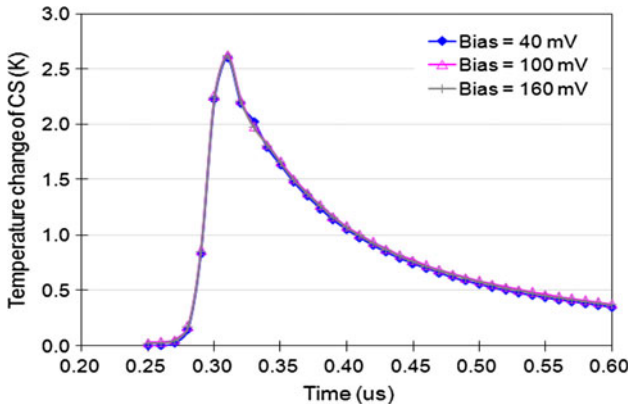

Fig. 7 Bias voltage effect on the temperature change of contact sensor

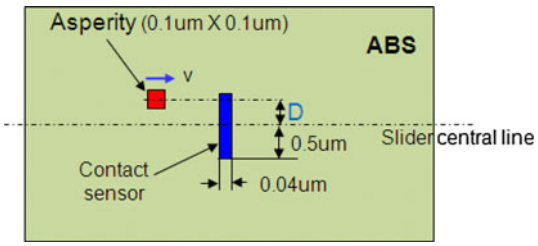

Fig. 8 Illustration of off-track definition

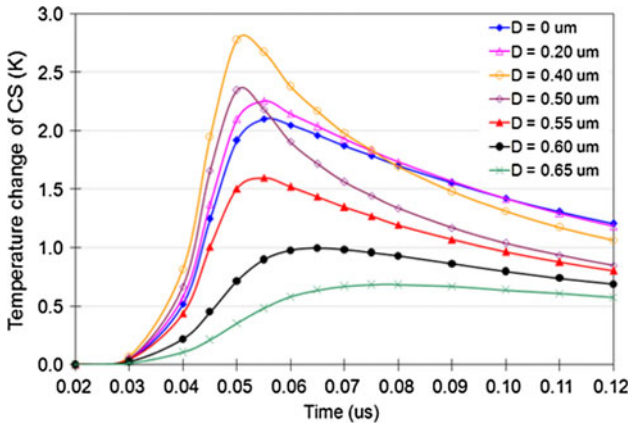

Fig. 9 Off-track effect on the temperature change of contact sensor

how the temperature of the contact sensor varies when there is margin between contacting point and the contact sensor. This session studies the cases where the margin is along the off-track direction.

As shown in Fig. 8, the off-track (D) is defined as the distance between central lines of the contact sensor and the asperity in slider width direction. For the analyses, the asperity size w is 100 nm, the normal pressure is 5 GPa and the sliding velocity is 10 m/s.

Figure 9 shows temperature change of the contact sensor with varying off-track (D) values, and Fig. 10 is the relative

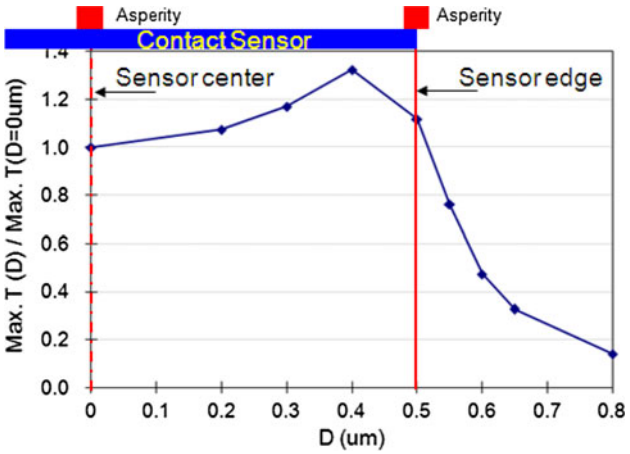

Fig. 10 Relative temperature variation

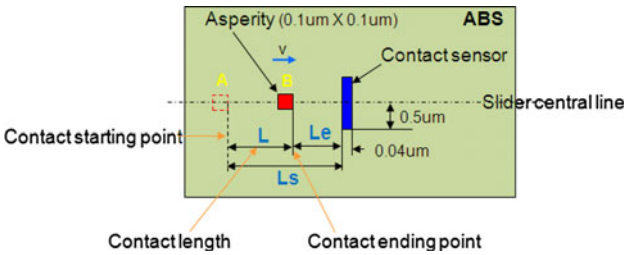

Fig. 11 Illustration of down-track definition

temperature change, where the reference is the temperature of the contact sensor with $D = 0$ μm. From the figure, it is observed that for $D \leq 0.50$ μm, the temperature of the contact sensor increases compared to $D = 0$ μm, it may be due to smaller thermal conductivity of the alumina. For $D \geq 0.55$ μm, there is no contact between the asperity and the contact sensor, the temperature rise of the contact sensor comes from heat transfer from the alumina, it quickly reduces with increasing off-track value.

3.8 Down-track effect

The margin between the contact point and the contact sensor may be along the down-track direction. The definition of down-track is illustrated in Fig. 11. Suppose the asperity starts to contact ABS at location A, and ends contact at location B. The distance from the contact starting point to contact ending point is denoted as contact length L, the distance from the contact starting point to the contact sensor is denoted as Ls, and the distance from the contact ending point to the contact sensor is denoted as Le.

From the down-track definition, two cases can be differentiated: (1) Constant contact length with different contact starting point, which means L is a constant value and Ls or Le is varying. From Eq. (1), the total dissipation

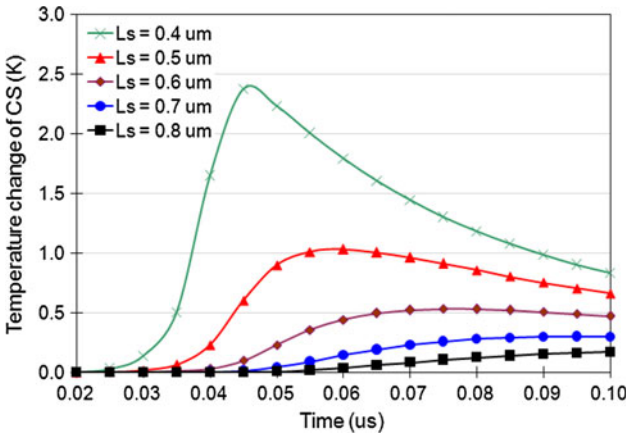

Fig. 12 Down-track effect on the temperature change of contact sensor

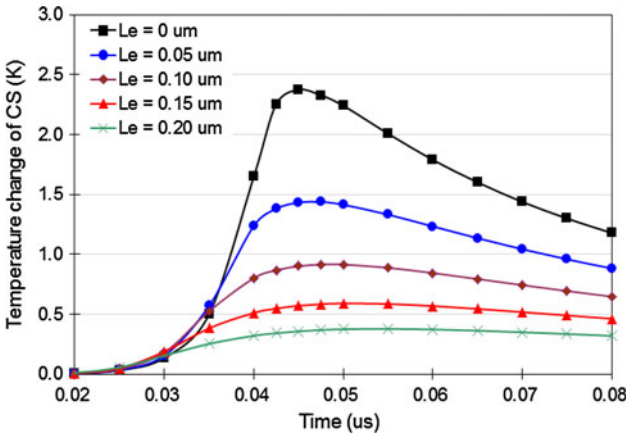

Fig. 14 Down-track effect on the temperature change of contact sensor

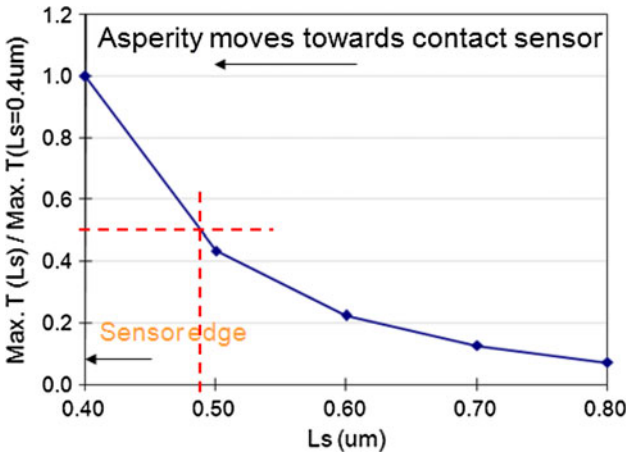

Fig. 13 Relative temperature variation

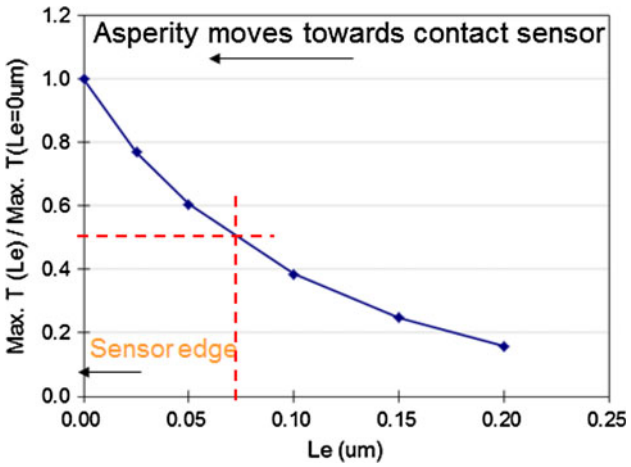

Fig. 15 Relative temperature variation

energy is the same for this case. (2) Varying contact length with the same contact starting point, which means Ls is the same but L or Le is varying. The total dissipation energy is different for this case.

3.8.1 Constant contact length

If we take the contact length $L = 0.4$ μm, and compare temperature at the contact sensor with varying contact starting point, Ls = 0.4 ∼ 0.8 μm or Le = 0∼0.4 μm. Figure 12 shows temperature change of the contact sensor with varying Ls value. Where the asperity size w is taken to be 100 nm, the normal pressure is 5 GPa and the sliding velocity is 10 m/s.

For Ls = 0.4 μm, the ending point is at the edge of the contact sensor, and there are no contact between the asperity and the sensor for Ls > 0.4 μm. The temperature rise of the contact sensor comes from the heat transfer from the alumina. It rapidly reduces with increasing Ls value.

Figure 13 shows the relative maximum temperature change of the contact sensor, where the reference temperature is the temperature of the contact sensor with Ls = 0.4 μm. It is observed that the temperature of the contact sensor drops 50 % when the Ls is about 0.48 μm or Le is 0.08 μm from the contact sensor edge. Thus, the contact ending point should be as close to the contact sensor as possible in order to get strong signal in the contact sensor.

3.8.2 Varying contact length

Next we suppose the contact starting point Ls = 0.4 μm, and compare temperature at the contact sensor with varying contact length, L = 0.2 ∼ 0.4 μm, or Le = 0∼0.2 μm. Figure 14 shows the temperature change of the contact sensor with varying Le value, where the asperity size w is taken to be 100 nm, the normal pressure is 5 GPa and the sliding velocity is 10 m/s.

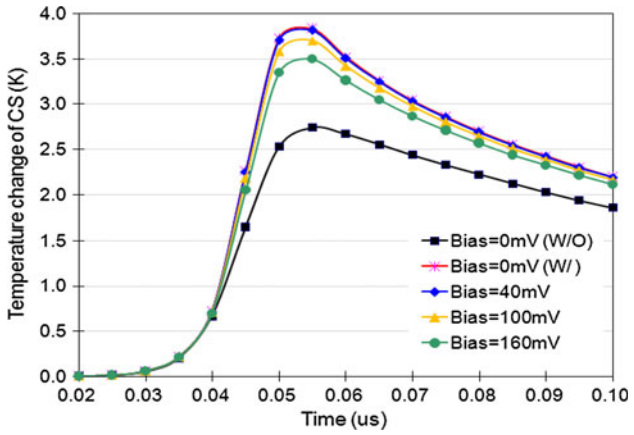

Fig. 16 Thermal contact conductance effect on the temperature change of the contact sensor

Figure 15 shows the relative temperature change of the contact sensor, where the reference is the temperature of the contact sensor with Le = 0 μm. It is shown that the temperature of the contact sensor quickly reduces with increasing Le value. It drops 50 % when the ending point is about 0.075 μm away from the contact sensor. For all these cases, there is also no direct contact between the asperity and the contact sensor.

3.9 Thermal contact conductance effect

For all the above analyses, it is supposed that there is no thermal contact conductance effect between the asperity and the contact sensor. But in actual cases, the heat could be transferred between the contacting surfaces.

In ANSYS, one way to model conduction is using a real constant TCC. The conductive heat transfer between two contacting surfaces is defined by (ANSYS Inc 2009; Lienhard 2000; Mikic and Rohsenow 1966):

$$q = TCC \times (T_t - T_c) \tag{3}$$

where q is the heat flux per area, TCC is called the thermal contact conductance coefficient, having units of heat/(time*temperature*area). T_t and T_c are the temperatures of the contact points on the target and contact surface.

Thermal contact conductance is a complicated phenomenon, influenced by many factors, such as contact pressure, interstitial materials, surface roughness, surface deformations and surface cleanliness. Since in this work, we are only focused on the effect of the thermal contact conductance. For simplicity, the thermal contact conductance coefficient between the asperity and the contact sensor is taken to be 18.0E + 6 and that between the asperity and the alumina is 1.0E + 6.

Figure 16 shows the contact conductance effect on the temperature change of the contact sensor. In the figure, the bias voltage effect is also included since it influences the temperature of the contact sensor. The case indicated as "W/O" means the thermal contact conductance effect is not taken into account, and the case indicated as "W/" means the thermal contact conductance effect is included in the simulation. The cases with bias voltage of 40 mV, 100 mV and 160 mV include the thermal contact conductance effect. Comparing the cases of "W/O" and "W/", it is observed that the temperature change of the contact sensor increases about 1 K when the thermal contact conductance is considered because heat can be transferred from the asperity to the contact sensor. From the figure, it is also shown that the temperature change of the contact sensor reduces with higher bias voltage. This is because more heat transfers from the contact sensor to the contacting asperity with higher temperature of the contact sensor.

4 Conclusions

A finite element contact model has been developed to study the signal variation in the contact sensor in hard disk drive for mapping asperities on disk surface. Parametric studies were carried out to investigate parameters' effect on the temperature change of the contact sensor, and the results can be summarized as follows:

- Cooling from air bearing reduces the temperature of the contact sensor about 15 % compared to without considering air bearing cooling effect
- Contact sensor temperature linearly increases with normal pressure, friction coefficient and asperity size
- Bias voltage effect on the temperature change of the contact sensor is negligible
- Sliding velocity effect becomes non-linear due to varying contact time
- By off-track and down-track analyses, the contacts should happen as close to the contact sensor as possible, especially in the down-track direction
- Contact sensor temperature increases when considering thermal contact conductance effect

The above simulation method and results can be a guideline for studying and developing a thermal contact sensor in the hard disk drive in order to further increase the area density.

References

ANSYS, Inc (2009) "Contact technology guide", Release 12.0
Barber JR (1967) The distribution of heat between sliding surfaces. J Mech Eng Sci 9:351–354
Barber JR (1970) The conduction of heat from sliding solids. Int J Heat Mass Transf 13:857–869

Kurita M, Xu J, Tokuyama M (2005) Flying-height reduction of magnetic head slider due to thermal protrusion. IEEE Trans Magn 41(5):3007–3009

Lienhard JH (2000) "A heat transfer textbook," 4th Edition, Phlogyston Press, Cambridge, Massachusetts

Mikic BB, Rohsenow WM (1966) "Thermal contact resistance", M.I.T. Dept. of Mechanical Engineering, Cambridge, Massachusetts

Nayak UV, Lee CK, O'Sullivan TC (2003) An overview of glide testing. IEEE Trans Magn 39(2):729–734

Persson BNJ (2000) Sliding friction: physical principles and applications, 2nd edn. Springer, Heidelberg

Shimizu Y, Xu J, Kohira H (2011) Nano-scale defect mapping on a magnetic disk surface using a contact sensor. IEEE Trans Magn 47(10):3426–3432